An innovative methodology for online surrogate-based model updating of historic buildings using monitoring data

Enrique García-Macías[a,*], Laura Ierimonti[a], Ilaria Venanzi[a], Filippo Ubertini[a]

[a]*Department of Civil and Environmental Engineering, University of Perugia, Via G Duranti 93, Perugia 06125, Italy*

Abstract

Structural Health Monitoring (SHM) based on Automated Operational Modal Analysis (A-OMA) has gained increasing importance in the conservation of heritage structures over recent decades. In this context, finite element model updating techniques using modal data constitute a commonly used approach for damage identification. Nevertheless, the large number of simulations usually involved in the associated minimization problem hinders the application to real-time condition assessment. This is specially critical for historic buildings, where the modelling of complex geometries involves large computational burdens. Alternatively, surrogate models offer an efficient solution to replace computationally demanding numerical models and so perform continuous model updating. In this light, this paper presents a surrogate-based model updating approach for online assessment of historic buildings and its application to a medieval masonry tower, the Sciri Tower in Perugia (Italy). Using modal properties identified by A-OMA, the proposed approach allows the continuous fitting of certain damage-sensitive parameters of the structure. To do so, three different surrogate models are considered, including the quadratic response surface method, Kriging, and Random Sampling High Dimensional Model Representation, and their effectiveness is compared from an SHM perspective. The reported results demonstrate the suitability of the proposed methodology for tracking temperature-dependent intrinsic properties of the tower.

Keywords: Damage Identification, Historic buildings, Operational Modal Analysis, Sciri Tower, Structural health monitoring, Surrogate models

1. Introduction

The vulnerability of cultural heritage buildings to ageing deterioration, climate change and extreme natural events, as well as their manifold cultural and economic values, make the use of non-destructive testing and preventive conservation a major concern for citizens and policy-makers in the European Union. In particular, masonry towers constitute specially vulnerable assets due to their high slenderness and mass, therefore their seismic risk assessment poses a priority issue [1]. Proof of this are the numerous collapses occurred during recent seismic events in Italy such as the 2009 M_w 6.3 L'Aquila earthquake [2], 2012 M_w 5.9 Emilia Romagna earthquake [3], or the 2016 M_w 6.5 Norcia earthquake [4]. In this context, SHM techniques based on OMA have proved to provide an efficient solution to interrogate the integrity of structures, along with damage identification tools suitable for condition-based maintenance and decision making [5, 6]. These techniques exploit ambient vibration records during in-service conditions to extract the modal features of the system, namely the natural frequencies, mode shapes, and damping ratios (see e.g. [7–10]). Given that these quantities depend upon the mass and stiffness distribution of the structure, the modal features can be tracked in time through long-term SHM systems and, thereby, damage can be related to their permanent variations. Furthermore, such systems can be scaled to building ensembles where several structures are simultaneously monitored in order to perform regional seismic risk assessment. In this way, after a seismic event, inspection and retrofit activities can be expeditiously scheduled prioritizing those buildings where damage poses a more severe risk to safety.

Vibration-based SHM techniques are eminently efficient for damage detection and, to some extent, damage quantification in the form of permanent variations in natural frequencies [11, 12]. Nevertheless, damage localization usually requires the inverse calibration of a finite element model (FEM) of the structure, also called FEM updating. This procedure aims to minimize the mismatch between the FEM response and certain experimental measurements (typically natural frequencies and mode shapes) by the calibration of the model parameters (e.g. material properties, connectivity, or boundary conditions). Thus, alterations of the modal features can be related to

*Corresponding author.
Email address: enrique.garciamacias@unipg.it (Enrique García-Macías)

damage-induced variations in the mechanical parameters of the structure and so identify the damage [13, 14]. Nonetheless, given the complexity that characterizes the geometry of most historic buildings, along with the large number of simulations that are usually required in the minimization problem associated with the FEM updating, the computational burden poses a major limitation in practice. This is particularly critical in masonry towers, which are usually surrounded by adjacent buildings conditioning their modal properties. While some research works report the successful application of simplified models of tower-building aggregate interactions through sets of elastic springs (see e.g. [15, 16]), such simplifications result inaccurate in many cases so that the adjoining buildings have to be included in the modelling. Alternatively, the use of computationally efficient surrogate models offers great potential to bypass time demanding numerical models when performing damage localization or continuous model updating. In this way, the surrogate model can be trained using a fully detailed FEM in a preliminary stage and, on this basis, the model updating procedure for damage identification can be conducted in a computationally inexpensive way. While some promising results have been reported in the realm of civil or aircraft structures, application studies to historic masonry structures are sorely lacking.

Model updating algorithms can be divided into two categories [17]: direct methods and iterative techniques. Direct methods update the mass and stiffness matrices directly based on the equations of motion of the system and the orthogonality of the mode shapes. While computationally inexpensive, these techniques cannot guarantee the symmetry and positive definiteness of the matrices, what hinders their physical description. On the other hand, iterative techniques progressively reduce the mismatch between the experimental and numerical responses until the updating parameters converge or the error function drops below a tolerance level [18]. These methods are further divided into two types [17], including gradient-based methods and evolutionary algorithms (i.e. genetic algorithms, particle swarm optimization, bees algorithms, etc). Despite being computationally demanding, evolutionary algorithms have superior capabilities to find global extrema under the presence of non-linearities, damping, measurement errors, as well as a large number of updating parameters [19]. Some application examples of these techniques to historic masonry structures can be found in the literature. For instance, Cavalagli *et al*. [20] used a derivative-free pattern search algorithm for the updating of a three-dimensional FEM of the San Pietro bell-tower in Perugia, Italy. Their results showed that the updated FEM on the basis of ambient-vibration tests (AVTs) could reproduce the damage experienced by the tower during the 2016 Central Italy seismic sequence. It is also worth noting the work by Gentile and Gallino [21] who updated a FEM of a historic suspension footbridge in Varallo Sesia (Italy) on the basis of an AVT and a gradient-based optimization technique. Ramos *et al*. [22] investigated the Mogadouro Clock Tower in Portugal and the effects of consolidation works carried out in 2005. By using two dynamic modal identification tests before and after the structural rehabilitation, those authors could identify the presence of severe damage in central parts of the south, east and west faades and at the upper part of the tower through a FEM updating process. Altunişik *et al*. [23] reported an automated FEM updating of an armory building located in Trabzon (Turkey) based upon the minimization of the differences between experimental and numerical natural frequencies. Pachón and co-authors [24] conducted the model updating of a three-dimensional FEM of the historical E. Torroja's bridge in the city of Córdoba (Spain) on the basis of experimentally identified modal properties and a genetic optimization algorithm.

As previously mentioned, the main drawback of evolutionary algorithms refers to the large number of function evaluations that are required to reach convergence and, given the complexity often involved in the modelling of masonry structures, this results in large computational costs. As a solution, surrogate-assisted evolutionary strategies propose the use of efficient models, such as response surface models (RSMs) [25], high-polynomial functions [26], or Kriging models [27] to approximate the objective function. Such meta-models explicitly describe the relationship between FEM responses and structural parameters in a computationally efficient way. In this line, only a few experiences can be found in the literature on the application to model updating of historical structures. It is worth noting the work by Cabboi *et al*. [25] who conducted an automated surrogate-based model updating of the San Vittore bell-tower in Milan (Italy). On the basis of continuous OMA, those authors used the RSM for the real-time updating of a 3D FEM of the tower. Similarly, Torres *et al*. [28] proposed a RSM-based FEM updating of the Metropolitan Cathedral of Santiago (Chile). Using an AVT and a gradient-based optimization method, those authors fitted the elastic parameters of a FEM by minimizing the differences between the experimental and numerical natural frequencies. The model updating approach based upon the combination of the RSM and a differential evolution algorithm proposed by Vincenzi and Savoia [26] was used by Bassoli *et al*. [29] for the model updating of a FEM of the San Felice sul Panaro medieval fortress in Modena (Italy). Their results demonstrated the capability of the surrogate-based model updating approach for the identification of the damage patterns experienced by the structure during the Emilia earthquake in 2012 in the shape of localized variations in the elastic parameters of the FEM.

This paper proposes an innovative surrogate-based model updating approach for real-time structural assessment of historical buildings. Using experimentally identified modal properties through A-OMA, the proposed methodology allows the continuous fitting and tracking of certain damage-sensitive parameters of the structure.

The Sciri Tower located in the city of Perugia (Italy) is used as a validation case study. The tower is inserted into a complex building ensemble with strong constraints on its modal properties, thereby the FE modelling requires the incorporation of the neighbouring buildings and a large mesh density. Therefore, this case study exemplifies the need for computationally efficient surrogate models for FEM updating applications. Firstly, the training population used for the construction of the surrogate models is generated through Monte Carlo simulations using a fully detailed 3D FEM. To do so, the FEM has been parametrized by dividing the geometry into four macro-elements with parametric elastic properties. Based upon this parametrization, three different surrogate models are built, including the RSM, Kriging, and Random Sampling High Dimensional Model Representation (RS-HDMR), and their effectiveness is evaluated by comparing their estimates of the modal features (resonant frequencies and mode shapes) against those obtained with the 3D FEM. Finally, the capability of the surrogate models to continuously assess the condition of the tower has been also analysed. To this aim, a continuous AVT has been conducted since 13$^{\text{th}}$ February until 10$^{\text{th}}$ March 2019 in order to identify the modal features of the tower and the environmental temperature. Then, the design parameters have been continuously fitted by minimizing the mismatch between the identified modal features and the estimates of the surrogate models. The results demonstrate the capability of the proposed approach to accurately reproduce the positive correlation of the stiffness of the structure with temperature. In addition, the Kriging model is shown superior for reproducing low temperature sensitivities although moderate or large training sample sizes are required. Conversely, while less accurate for small sensitivities, the RSM and RS-HDMR surrogate models are reported to provide computationally efficient tools with great potential for conducting rapid structural assessment.

The remaining of this paper is organized as follows. Section 2 concisely overviews the three studied surrogate models. Section 3 presents the proposed surrogate-based model updating approach for continuous damage assessment of historic structures. Section 4 reports the validation case study and discussion and, finally, Section 5 concludes the paper.

2. Theoretical background: surrogate modelling

In this section, the three considered surrogate models are concisely overviewed, namely the RSM, Kriging, and RS-HDMR models. In general, the purpose of a surrogate model is to bypass in a cost-effective way the Input/Output relationship of a computationally demanding model. Let us define m damage-sensitive parameters, $x_i \in \mathbb{R}$, $i = 1, ..., m$, determining the response y of a FEM. A surrogate model has to provide a black-box representation of the response of the main model as $y(\mathbf{x})$, with $\mathbf{x}$ being the vector of design parameters $\mathbf{x} = [x_1, ..., x_m]^{\mathrm{T}}$. To do so, it is often necessary to obtain a training population. This consists of a set of N input-output samples obtained by direct Monte Carlo simulations using the main FEM in order to map the output y and the design space of the input parameters x_i. In formal terms, a training population is defined by the matrix of design sites $\mathbf{X}=[\mathbf{x}^1, \ldots, \mathbf{x}^N]$ with dimensions $m \times N$, and the observation vector $\mathbf{Y}=[y_1, \ldots, y_N]^{\mathrm{T}}$, with $y_i \in \mathbb{R}$ being the system's response to the input x_i. In this work, the modal properties obtained by a linear modal analysis of the FEM are assumed as outputs. Therefore, a different surrogate model must be constructed for each natural frequency and modal amplitude of all the vibration modes considered in the analysis. Specifically, if l modes of vibration are selected and n^{dof} degrees of freedom are used to sample the mode shapes, a total of $l\,(1 + n^{dof})$ surrogate models must be constructed, including l models to represent the resonant frequencies, and $l \cdot n^{dof}$ to reproduce the modal amplitudes.

2.1. Response Surface Method (RSM)

The RSM is a collection of statistical techniques used for fitting empirical models and so reduce the computational effort in iterative processes [30]. In this work, a second-order quadratic version of the RSM is used as [31]:

$$y(\mathbf{x}) = \alpha_0 + \sum_{j=1}^{m} \alpha_j x_j + \sum_{j=1}^{m} \alpha_{jj} x_j^2 + \sum_{j=1}^{m} \sum_{i \geq j}^{m} \alpha_{ji} x_j x_i + \epsilon, \tag{1}$$

with coefficients α_0, α_j, α_{jj} and α_{ji} being the intercept, linear, quadratic, and interaction coefficients, respectively. The term ϵ accounts for all those variability sources not included in the fitting, such as measurement error in the response, background noise, non-considered variables, etc. Typically, ϵ is treated as a statistical error, often assuming it to be normally distributed with zero mean, independent and identically distributed at each observation. The model in terms of the observations included in the training population of N individuals can be written in matrix notation as:

$$\mathbf{Y} = \hat{\mathbf{X}}\mathbf{A} + \boldsymbol{\epsilon}, \tag{2}$$

where $\hat{\mathbf{X}}$ is a $N \times (m+1)(m+2)/2$ matrix collecting components $[1, x_j, x_j^2, x_j x_i]$ for each individual in the training population, $\mathbf{A}$ is the $(m+1)(m+2)/2$ vector of coefficients α_0, α_j, α_{jj} and α_{ji}, and $\boldsymbol{\epsilon}$ is a $(m+1)(m+2)/2$ vector of random errors. The meta-model is constructed by obtaining the coefficients vector $\mathbf{A}$, which is usually determined by its least squares estimator as [32]:

$$\mathbf{A} = \left(\hat{\mathbf{X}}^{\mathrm{T}}\hat{\mathbf{X}}\right)^{-1} \hat{\mathbf{X}}^{\mathrm{T}}\mathbf{Y}, \tag{3}$$

whereby the fitted regression model reads:

$$\mathbf{Y} = \hat{\mathbf{X}}\mathbf{A}. \tag{4}$$

2.2. Kriging model

The Kriging model, with origin in Geostatistics [33], is a commonly used technique of interpolation for spatial data. The Kriging interpolator conceives the function of interest $y(\mathbf{x})$ as the sum of a regression model $y_r(\mathbf{x})$ and a random function $\mathcal{F}(\mathbf{x})$ with zero mean as follows [34]:

$$y(\mathbf{x}) = y_r(\mathbf{x}) + \mathcal{F}(\mathbf{x}). \tag{5}$$

It can be understood that $y_r(\mathbf{x})$ globally approximates the design space, whilst $\mathcal{F}(\mathbf{x})$ introduces localized deviations. The regression function $y_r(\mathbf{x})$ depends upon p regression parameters $\boldsymbol{\beta}=\left[\beta_1, \ldots, \beta_p\right]$, and given functions $\mathbf{f}(\mathbf{x})=\left[f_1(\mathbf{x}), \ldots, f_p(\mathbf{x})\right]$ with $f_i : \mathbb{R}^m \to \mathbb{R}$, as [34]:

$$y_r(\boldsymbol{\beta}, \mathbf{x}) = \mathbf{f}^{\mathrm{T}}(\mathbf{x})\boldsymbol{\beta}. \tag{6}$$

The covariance matrix of $\mathcal{F}(\mathbf{x})$ between any two of the N-sampled data points $\mathbf{x}_i$ and $\mathbf{x}_j$ reads:

$$\mathrm{Cov}\left[\mathcal{F}(\mathbf{x}_i)\mathcal{F}(\mathbf{x}_j)\right] = \sigma^2 \mathbf{R}\left[r(\boldsymbol{\theta}, \mathbf{x}_i, \mathbf{x}_j)\right], \tag{7}$$

where σ^2 stands for the variance of $\mathcal{F}(\mathbf{x})$, and $r(\boldsymbol{\theta}, \mathbf{x}_i, \mathbf{x}_j)$ is a given spatial correlation function between $\mathbf{x}_i$ and $\mathbf{x}_j$ and dependent on $\boldsymbol{\theta}$ correlation parameters. Finally, the term $\mathbf{R}$ is a $N \times N$ symmetric, positive definite matrix with components $R_{ij} = r(\boldsymbol{\theta}, \mathbf{x}_i, \mathbf{x}_j)$.

The relation between the interpolated values $\hat{y}(\mathbf{x})$ of the response $y(\mathbf{x})$ at an arbitrary design site $\mathbf{x}$ is defined by the Kriging predictor as follows:

$$\hat{y}(\mathbf{x}) = \mathbf{f}^{\mathrm{T}}(\mathbf{x})\boldsymbol{\beta} + \mathbf{r}(\mathbf{x})^{\mathrm{T}}\mathbf{R}^{-1}\left[\mathbf{Y} - \mathbf{f}^{\mathrm{T}}(\mathbf{x})\boldsymbol{\beta}\right], \tag{8}$$

where $\mathbf{r}(\mathbf{x})$ is a vector containing the correlations between the design sites and $\mathbf{x}$ as:

$$\mathbf{r}(\mathbf{x})^{\mathrm{T}} = \left[r(\boldsymbol{\theta}, \mathbf{x}_1, \mathbf{x}), \ldots, r(\boldsymbol{\theta}, \mathbf{x}_m, \mathbf{x})\right]^{\mathrm{T}}. \tag{9}$$

Hence, once the regression model and the correlation function are chosen, the Kriging interpolator is constructed by selecting adequate regression parameters $\boldsymbol{\beta}$ and correlation parameters $\boldsymbol{\theta}$. In this work, Gaussian correlation functions and zero-th order regression functions are selected.

2.3. Random Sampling High-Dimensional Model Representation (RS-HDMR)

Random sampling high dimensional model representation (RS-HDMR) constitutes a set of tools originally proposed by Rabitz *et al.* [35] for approximating high-dimensional input-output systems based on a linear combination of basis functions with increasing order [36]. In this method, all the input variables are rescaled in the range $[0, 1]$, thereby the output function is defined in a unit hypercube $K^m = \{(x_1, \ldots, x_m) | \, 0 \leq x_i \leq 1, \, i = 1, , m\}$. The relationship between the input $\mathbf{x}$ and the output $y(\mathbf{x})$ variables can be expressed by HDMR as [36]:

$$y(\mathbf{x}) = f_0 + \sum_{i=1}^{m} f_i(x_i) + \sum_{1 \leq i < j \leq m} f_{ij}(x_i, x_j) + \ldots + f_{12\ldots m}(x_1, x_2, \ldots, x_m), \tag{10}$$

here, the term f_0 is a scalar function relating the mean contribution of all the inputs to the output $y(\mathbf{x})$. Functions $f_i(x_i)$ are first-order terms giving the effect of variable x_i acting independently upon the output, and $f_{ij}(x_i, x_j)$ are second-order terms describing the cooperative effects of two input variables x_i and x_j. Higher order terms can be successively defined accounting for the cooperative effect of an increasing number of input variables on $y(\mathbf{x})$. Nonetheless terms up to second-order suffice to provide accurate results in most cases [36]. The last term $f_{(12\ldots m)}(x_1, x_2, \ldots, x_m)$ stands for the residual m-th order contribution of all the input variables, and it is evaluated

as the difference between $f(\mathbf{x})$ and all the other component functions. The component functions in Eq. (10) are determined through an averaging process as follows [37]:

$$f_0 = \int_{K^m} y(\mathbf{x})\,\mathrm{d}x \approx \frac{1}{N}\sum_{s=1}^{N} y(\mathbf{x}^s), \tag{11a}$$

$$f_i(x_i) = \int_{K^{m-1}} y(\mathbf{x})\,\mathrm{d}x^i - f_0, \tag{11b}$$

$$f_{ij}(x_i, x_j) = \int_{K^{m-2}} y(\mathbf{x})\,\mathrm{d}x^{ij} - f_i(x_i) - f_0, \tag{11c}$$

where $\mathrm{d}x^i$ stands for the product $\mathrm{d}x_1\,\mathrm{d}x_2 \ldots \mathrm{d}x_n$ without $\mathrm{d}x_i$, whereas $\mathrm{d}x^{ij}$ denotes the same product without $\mathrm{d}x_i$ and $\mathrm{d}x_j$. The component functions can be further approximated by orthonormal basis functions $\varphi_r(x_i)$, $\varphi_p(x_i)$, and $\varphi_q\left(x_j\right)$ as:

$$f_i(x_i) \approx \sum_{r=1}^{o_1} \alpha_r^i\,\varphi_r(x_i), \tag{12a}$$

$$f_{ij}(x_i, x_j) \approx \sum_{p=1}^{o_2}\sum_{q=1}^{o_3} \beta_{pq}^{ij}\,\varphi_p(x_i)\,\varphi_q(x_j), \tag{12b}$$

where o_1, o_2, and o_3 represent the orders of the functions $\varphi_r(x_i)$, $\varphi_p(x_i)$, and $\varphi_q\left(x_j\right)$. The expressions of the orthonormal polynomials are determined by the conditions of zero mean, unit norm and orthogonality in the domain $[0, 1]$. For more specific information in this regard, readers can refer to reference [38]. The expansion coefficients α_r^i and β_{pq}^{ij} are scalars to be determined. To do so, the integrals in Eq. (11) can be approximated by Monte Carlo summations over the training population, leading to:

$$\alpha_r^i \approx \frac{1}{N}\sum_{s=1}^{N} y(\mathbf{x}^s)\,\varphi_r\left(x_i^s\right), \tag{13a}$$

$$\beta_{pq}^{ij} \approx \frac{1}{N}\sum_{s=1}^{N} y(\mathbf{x}^s)\,\varphi_p\left(x_i^s\right)\varphi_q\left(x_j^s\right), \tag{13b}$$

and the final expression of the RS-HDMR model with component functions up to second-order takes the form:

$$y(\mathbf{x}) = f_0 + \sum_{i=1}^{m}\sum_{r=1}^{o_1} \alpha_r^i \varphi_r(x_i) + \sum_{1\le i<j\le m}\sum_{p=1}^{o_2}\sum_{q=1}^{o_3} \beta_{pq}^{ij}\varphi_p(x_i)\varphi_q(x_j). \tag{14}$$

The accuracy of the fitting is determined by the Monte Carlo integration used for the estimation of the expansion coefficients α_r^i and β_{pq}^{ij}. Variance reduction methods such as the correlation [39] and ratio control variate [40] methods are often used to improve the accuracy of the integration. In both cases, the determination of the expansion coefficients is conducted in an iterative way and requires a reference function similar to $y(\mathbf{x})$, which is usually approximated as a truncated RS-HDMR expansion [37]. In this work, the GUI-HDMR toolbox for Matlab developed by Ziehn and Tomlin [36] is used. This toolbox implements an optimization method based on the least squares method to determine the best polynomial order for each of the component functions. In the subsequent results reported in Section 4, first and second order component functions are used with orthonormal polynomials up to second order, as well as the correlation method to improve the accuracy of the Monte Carlo integration.

3. Surrogate-based continuous assessment of historic structures

The proposed surrogate-based continuous model updating approach for the structural assessment of historic masonry buildings is sketched in Fig. 1. The procedure comprises five consecutive steps:

(A) *Identification of damage-sensitive parameters of the FEM of the structure.* These parameters constitute the design variables of the model updating, so that the parameter selection must be capable of reproducing the expected damage-induced stiffness variations.

(B) *Sampling of the design space.* On the basis of the previously selected parameters, the design space is uniformly sampled to generate a representative input data set.

(C) *Generation of the training population.* Considering the previously defined design space, the modal features of the structure are estimated by the FEM through Monte Carlo Simulations (MCS). This creates a mapping between the design variables and the numerical modal features of the structure that serves as the training data sample to construct the surrogate models.

(D) *Construction of the surrogate model.* The training population is used to estimate the parameters defining the selected surrogate model according to what described in previous section.

(E) *Continuous surrogate-based model updating*. Based upon the previously constructed surrogate model, the design variables are continuously fitted through a model updating approach. To do so, an optimization problem is set up to minimize the differences between experimentally and numerically identified modal features. Dividing the monitoring period into consecutive time steps, this process is defined in an iterative way, and the tracking of the fitted design variables provides a continuous assessment of the structure.

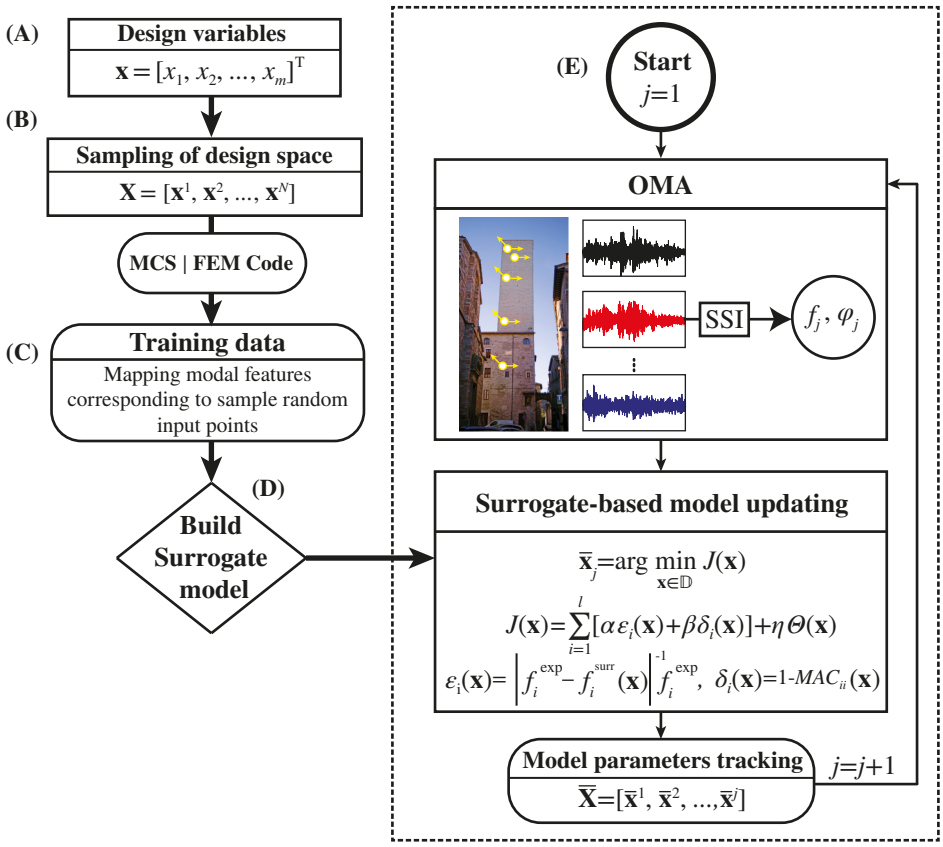

Figure 1: Flowchart of the proposed surrogate-based continuous structural assessment of historic buildings.

In this work, the design variables x_i are allowed to vary only within a certain range $[a_i, b_i]$, i.e. $a_i \leq x_i \leq b_i$. Therefore, the vector of design variables $\mathbf{x}$ is defined in an m-dimensional space $\mathbf{x} \in \mathbb{D}$ defined as $\mathbb{D} = \{\mathbf{x} \in \mathbb{R}^m : a_i \leq x_i \leq b_i\}$. Diverse variables x_i can be chosen such as the elastic properties and/or connectivity of some elements, boundary conditions or even topological parameters. The elastic moduli of certain parts of the FEM are selected herein as design variables as later explained in Section 4.3. Let us recall that a number of l natural frequencies and mode shapes are considered in the model updating, thence an objective function $J(\mathbf{x})$ including the differences between the experimental modal features and the predictions of the surrogate model can be introduced in step (E) as follows:

$$J(\mathbf{x}) = \sum_{i=1}^{l} \left[\alpha\varepsilon_i(\mathbf{x}) + \beta\delta_i(\mathbf{x})\right] + \eta\Theta(\mathbf{x}), \tag{15}$$

with

$$\varepsilon_i(\mathbf{x}) = \frac{\left|f_i^{\text{exp}} - f_i^{\text{surr}}(\mathbf{x})\right|}{f_i^{\text{exp}}}, \quad \delta_i(\mathbf{x}) = 1 - MAC_{ii}(\mathbf{x}), \tag{16}$$

and α and β weighting coefficients that modulate the importance of the first two terms of the objective function. The terms f_i^{exp} and $f_i^{\text{surr}}(\mathbf{x})$ stand for the i-th resonant frequencies obtained by OMA and the surrogate model, respectively. In addition, the terms MAC_{ii} are the Modal Assurance Criterion (MAC) coefficients between the i-th experimental φ_i^{exp} and numerical $\varphi_i^{\text{surr}}(\mathbf{x})$ mode shapes. Therefore, the model updating procedure is defined as the following constrained non-linear minimization problem:

$$\overline{\mathbf{x}} = \arg\min_{\mathbf{x}\in\mathbb{D}} J(\mathbf{x}). \tag{17}$$

The term $\Theta(\mathbf{x})$ in Eq. (15) stands for a regularization term used to reduce ill-conditioning limitations in the optimization. Such limitations imply that design variables at distinct locations of the search space may produce the same response and, hence, the solution cannot be affirmed as unique. In this work, a simple regularization term is incorporated as follows:

$$\Theta(\mathbf{x}) = \frac{1}{m}\sum_{i=1}^{m}\frac{\left(x_i - x_i^0\right)^2}{b_i - a_i}, \tag{18}$$

along with a trade-off parameter η to modulate the relevance of the regularization in the cost function in Eq. (15). The implemented regularization term imposes the solution to remain close to a reference vector of design variables $\mathbf{x}^0 = \left[x_1^0, ..., x_m^0\right]^{\text{T}}$ or an undamaged condition. For small values of η, the design variables are almost unrestricted and the optimization resembles the original ill-posed problem. Conversely, too large values of η may lead to over-constricted conditions and large disagreements between the experimental and numerical modal features. The selection of η depends upon the complexity of the structure and the chosen fitting parameters, thereby a tailored sensitivity analysis must be performed for each specific case. In this work, sensitivity analyses showed that a value of η=0.3 provides reasonably good solutions for the present case study of the Sciri Tower.

The modal features of the structure are experimentally obtained by A-OMA at consecutive time steps j. Therefore, the model updating procedure in Eq. (17) is iteratively performed, and the fitted design variables are collected in matrix form as $\overline{\mathbf{X}} = \left[\overline{\mathbf{x}}_1, ..., \overline{\mathbf{x}}_j\right]$. This provides a continuous assessment of the structure based on the tracking of the selected design variables, thereby the appearance of damage can be inferred in the shape of anomalies in the matrix $\overline{\mathbf{X}}$.

4. Validation case study and discussion

This section reports the validation of the previously introduced surrogate-based model updating approach with a case study of the Sciri Tower. Specifically, Section 4.1 describes the validation case study. Section 4.2 presents the ambient vibration testing and A-OMA conducted on the tower with the aim of continuously identifying its modal features. Afterwards, Section 4.3 details the FE modelling of the tower and its parametrization through damage-sensitive parameters. Finally, Sections 4.4 and 4.5 report the comparison of the considered surrogate models and their application for continuous structural assessment of the Sciri Tower, respectively.

4.1. The Sciri Tower

The proposed surrogate-based continuous model updating approach is validated with a case study of the 41 m high civic tower located in the historical centre of Perugia (Italy), named *Torre degli Sciri* (see Fig. 2 (a)). The Sciri Tower was erected in the late 13$^{\text{th}}$ century for defensive purposes and, nowadays, it is the only remaining medieval tower in a good state of preservation in the city of Perugia. The Sciri Tower forms part of a building ensemble with approximate plan dimensions of 22 × 25 m (see Fig. 2 (b)). Three façades of the tower are connected to the adjacent masonry buildings up to a height of 17 m, while the fourth one remains exposed. The tower has a hollow rectangular cross-section of 7.15 × 7.35 m and can be ideally divided into two structural portions. The lower part has wall thicknesses of 1.68 m and 2.1 m and rises up to 8.4 m. In this part, there are some small openings and a stone masonry vault standing above an old chapel. On the other hand, the upper part has slender continuous walls (with thickness varying in height from 1.6 m to 1.4 m), with four 1.5 m wide masonry vaulted slabs at different heights. A brick masonry ceiling vault completes the tower, and a 0.5 m thick parapet extends up to a total height of 41 m. The masonry of the tower consists of homogeneous and regular squared white limestone blocks.

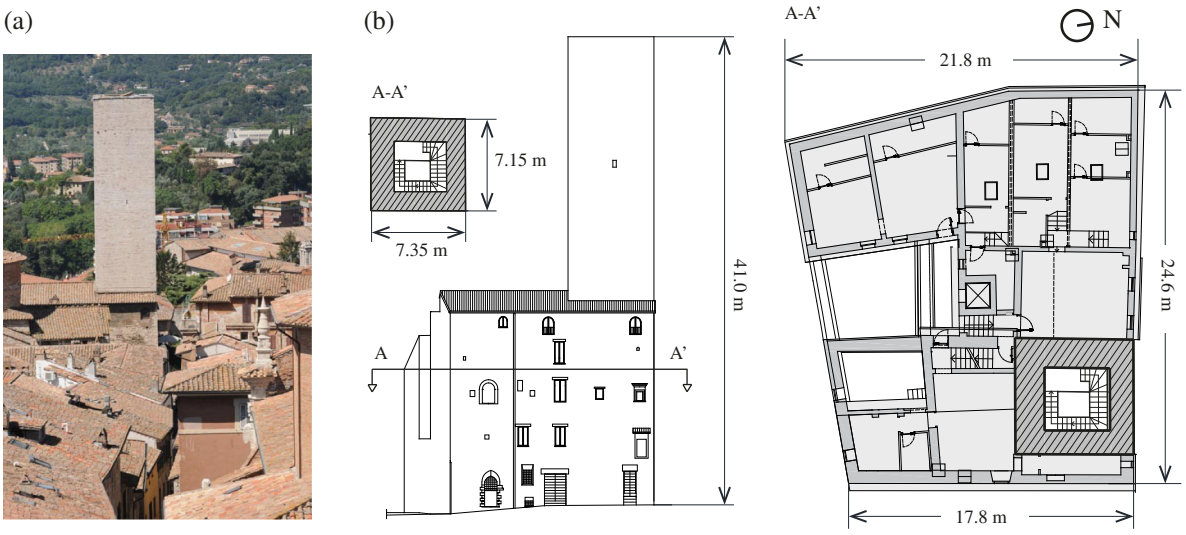

Figure 2: A photograph of the Sciri Tower (a), and elevation and plan views (b).

4.2. Ambient vibration testing and operational modal analysis

With the aim of identifying the modal features of the Sciri Tower, a continuous ambient vibration testing was performed for three weeks, since 13th February until 10th March 2019. To this end, a total of 12 high sensitivity (10 V/g) uniaxial PCB 393B12 accelerometers were installed at four different heights of the tower, namely z = 40.5 m, z = 33.5 m, z = 24.0 m and z = 8.4 m, as shown in Figure 3. The ambient vibrations induced by traffic, human and wind actions in operational conditions were recorded at a sampling frequency of 1652 Hz and later downsampled to 40 Hz. In addition, two K-type thermocouples were also installed at the level z = 40.5 m (indoor and outdoor) and temperature was recorded at a sampling frequency of 0.4 Hz. Field data were acquired using a multi-channel data acquisition system (DAQ) model NI CompactDAQ-9184 located at the level z = 36.7 m, equipped with NI 9234 data acquisition modules for accelerometers (24-bit resolution, 102 dB dynamic range and anti-aliasing filters) and NI 9219 modules for thermocouples (24-bit resolution, ±60 V range, 100 S/s). A LabView toolkit was implemented for data acquisition and preliminary real-time processing, including amplitude and spectral plots for quality-control inspections. Data were recorded in separate files containing 30-min long acceleration and temperature time series, and transferred in real-time through Wi-Fi connection to the Laboratory of Structural Dynamics of the University of Perugia, 2.5 km far from the tower. Here, data were stored and processed with the purpose of extracting the dynamic characteristics of the tower.

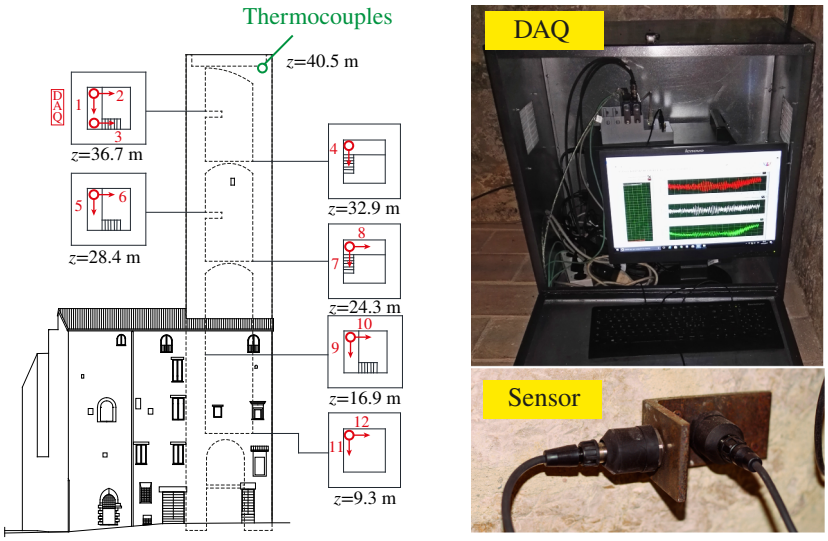

Figure 3: Sensors layout for continuous monitoring of the Sciri Tower.

The modal features of the tower have been identified by the Covariance driven Stochastic Subspace Identi-

fication (COV-SSI) method [41]. By means of a self-developed fully automated implementation in Matlab environment, the modal features have been continuously extracted from every 30-min long records. The modal features obtained from the first measurements, taken on 13th February 2019 at 14:00 UTC, have been used for an initial tuning of the FEM of the tower as shown later in Section 4.3. In particular, six vibration modes have been identified in the range between 0 and 10 Hz as shown in Fig 4, including two flexural modes in NW direction (x-direction, denoted as Fx1 and Fx2, respectively), two flexural modes in SW direction (y-direction, denoted as Fy1 and Fy2, respectively), one torsional mode, Tz1, and one higher order flexural mode, Fx3. Figure 5 shows the first four singular values of the power spectral density matrix of the acceleration records, where six resonant peaks are clearly identified. The obtained mode shapes are depicted in Fig. 4. In this figure, the identified mode shapes are also plotted in the polar plane, where each arrow represents a component of the mode shape vector. Normal (real) mode shapes have components with phases of 0 or 180°, while scatters in the complexity plot indicate complex mode shapes. Experimental mode shapes can be complex for a number of reasons: limitations in the identification of low-excited modes, modelling errors, or non-classically (proportionally) damped modes. It is noted in Fig. 4 that modes Fx1, Fy1, Tz1, and Fx3 are identified as real modes, while some scatter can be observed in the remaining modes, particularly in mode Fy2. The natural frequencies and damping ratios of the identified modes are reported in Table 1. In addition, in order to quantify the complexity of the modes, the Modal Phase Collinearity (MPC) [42] values are also reported. Values of MPC close to 100% indicate perfect mode shape collinearity, while lower values indicate increasingly complex modes. It is noted that the MPC of all the modes are above 95%, except for modes Fx2 and Fy2 where values of 84.9% and 80.2% are obtained, respectively. These results evidence that the comparison between the experimental and numerical (undamped) mode shapes for the vibration modes Fx2 and Fy2 may yield considerable discrepancies.

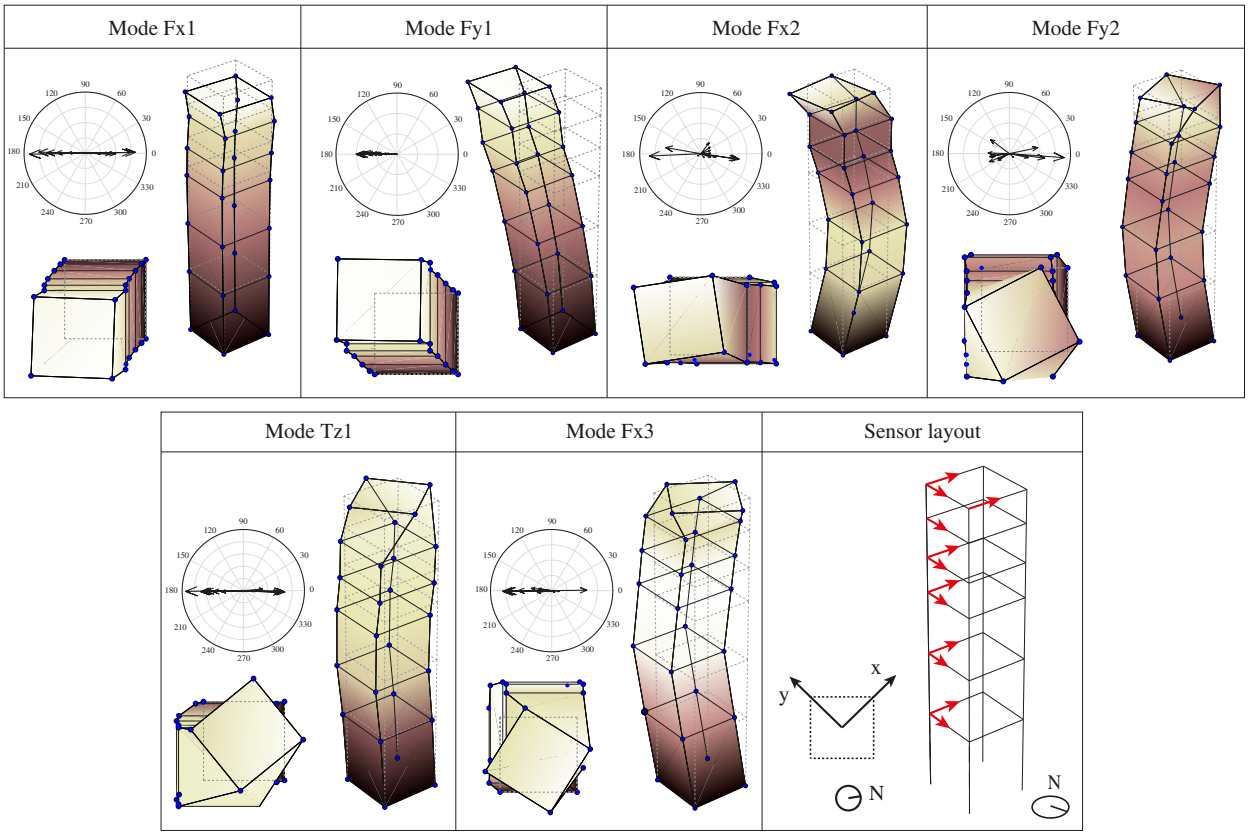

Figure 4: Experimentally identified mode shapes estimated through COV-SSI on 13th February 2019 at 14:00 UTC.

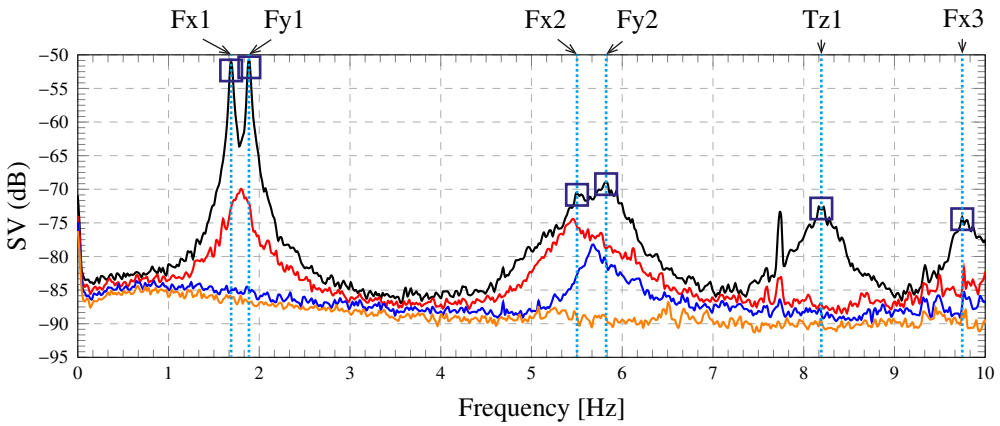

Figure 5: First four singular values (SV) of the power spectral density matrix obtained from the ambient vibrations recorded on 13th February 2019 at 14:00 UTC.

Table 1: Experimentally identified natural frequencies f_i^{exp}, damping ratios ζ_i and Modal Phase Collinearity (MPC) estimated through COV-SSI on 13th February 2019 at 14:00 UTC.

Mode	f_i^{exp} [Hz]	ζ_i [%]	MPC_i [%]
Fx1	1.692	0.918	99.8
Fy1	1.891	0.779	99.4
Fx2	5.539	3.066	84.9
Fy2	5.829	2.175	80.2
Tz1	8.205	1.783	99.8
Fx3	9.795	1.365	98.9

4.3. Finite Element Modelling

In order to generate a training population for building the surrogate models, a 3D FEM of the Sciri Tower and the surrounding buildings has been built using the commercial software ABAQUS 6.10 (see Fig. 6). The geometry of the model has been defined using available structural drawings and in-situ inspections, partitioning it into different regions to facilitate the materials assignment. Given that the FEM is used only to conduct linear modal analyses, all the materials in the model have been considered as elastic isotropic. The soil-structure interaction has been assumed negligible, thereby fixed boundary conditions have been defined at the ground level. Ten-node tetrahedral elements `C3D10` have been used for meshing the geometry with mean element size of about 50 cm. This brings to 245149 and 411140 the total number of elements and nodes, respectively, what justifies the use of a surrogate model to limit the computational burden involved in the subsequent model updating procedure. It is important to note that the use of simplified spring elements to simulate the restrains imposed by the adjoining buildings did not properly reproduce the experimentally identified modes of vibration, specially the torsional mode, whereby a detailed modelling of the neighbouring buildings became imperative.

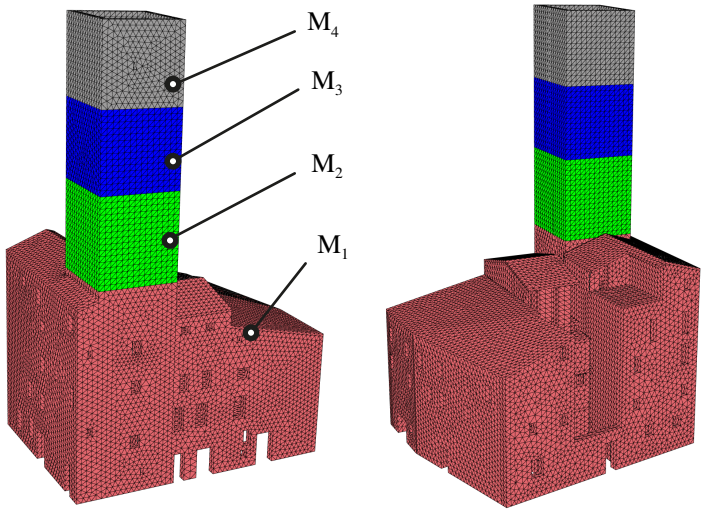

Figure 6: Finite element model of the Sciri Tower and the adjoining building, and division into macro-elements M_1, M_2, M_3 and M_4.

The initial mechanical parameters of the model have been defined according to the Italian technical standard code for square stone masonry, including the Young's modulus $E = 4.03$ GPa, shear modulus $G = 1.61$ GPa, Poisson's ratio $\nu = 0.25$, and mass density $w = 2.20$ t/m^3. Afterwards, in order to obtain consistent modal estimates with the experimental ones previously reported in Section 4.2, a thorough model calibration has been carried out through a sensitivity analysis. Specifically, eighteen different materials have been considered in the modelling, including the tower, as well as ten masonry walls, four floors, and three parts of the roof of the building aggregate. Table 2 shows the mechanical parameters of the tower before and after calibration. On this basis, Table 3 reports the comparison between the experimental and numerical modal features, and Fig. 7 shows the numerical mode shapes obtained from the linear modal analysis of the tuned FEM. Good agreements can be observed for modes Fx1, Fy1, Fx2, Tz1, and Fx3 with relative differences in terms of resonant frequencies below 5% and MAC values above 0.8. Conversely, larger discrepancies are noted for mode Fy2 with a relative difference in resonant frequency of 5.577%. The MAC values are also small in this case with a value of 0.108. In this particular mode of vibration, the low MAC value is ascribed to the high complexity of the experimental mode shape as previously reported in Fig. 4. The reported discrepancies may be also due to structural aspects disregarded in the modelling, such as the soil-structure interaction [43]. Nonetheless, further detailing of the FEM falls out the scope of this paper, and the accuracy achieved in Table 3 is considered sufficient for the purpose of the present investigation.

Table 2: Mechanical parameters of the FEM of the tower before and after calibration.

	Youngs' modulus E [kN/m^2]	Shear modulus G [kN/m^2]	Poisson's ratio ν [-]	Mass density w [t/m^3]
Before calibration	4.03e+06	1.61e+06	0.25	2.20
After calibration	5.77e+06	2.31e+06	0.23	2.20

Table 3: Comparison between experimental and numerical modal parameters after calibration.

Mode	f_i^{exp} [Hz]	f_i^{FEM} [Hz]	$\left(f_i^{\text{exp}} - f_i^{\text{FEM}}\right)/f_i^{\text{exp}}$ [%]	MAC [-]
Fx1	1.692	1.753	-3.655	0.972
Fy1	1.891	1.966	-3.970	0.960
Fx2	5.539	5.706	-3.019	0.802
Fy2	5.830	6.155	-5.577	0.108
Tz1	8.205	7.993	2.584	0.866
Fx3	9.795	9.822	-0.271	0.913

With the purpose of parametrizing the FEM for the proposed surrogate-based model updating approach, the elastic properties of certain regions of the structure have been defined as design variables. To do so, the tuned FEM has been subdivided into four macro-elements M_i, $i = 1, ..., 4$, as illustrated in Fig. 6. Macro-element M_1 includes

the adjoining building and a portion of the tower up to the top height of the roof of the building aggregate (0-18.9 m). Macro-elements M_2, M_3 and M_4 comprise the portions of the tower located between heights of 18.9-26.8 m, 26.8-33.8 m, and 33.8-41.0 m, respectively. According to this partition, the Young's modulus E_i of the elements contained in a generic macro-element M_i has been defined as a random variable as:

$$E_i = E_i^0 (1 + k_i), \tag{19}$$

with E_i^0 being the nominal value of the Young's modulus of the i-th macro-element. Note that E_1^0 defines the nominal Young's modulus of the first section of the tower, as well as the moduli of the different partitions of the adjoining building (see Fig. 6). The parameters k_i are random linear proportionality coefficients of the elastic moduli of macro-elements M_i, and represent the design variables $\mathbf{x} = [k_1, k_2, k_3, k_4]^T$ in the model updating approach previously introduced in Eq. (17). On this basis, larger permanent reductions in one component of $\mathbf{x}$ with respect to the others would indicate the presence of damage in the corresponding macro-element. Additionally, as shown below in Section 4.5, this parametrization is also suitable for accounting for environmental effects, specifically the influence of temperature on the stiffness distribution of the structure.

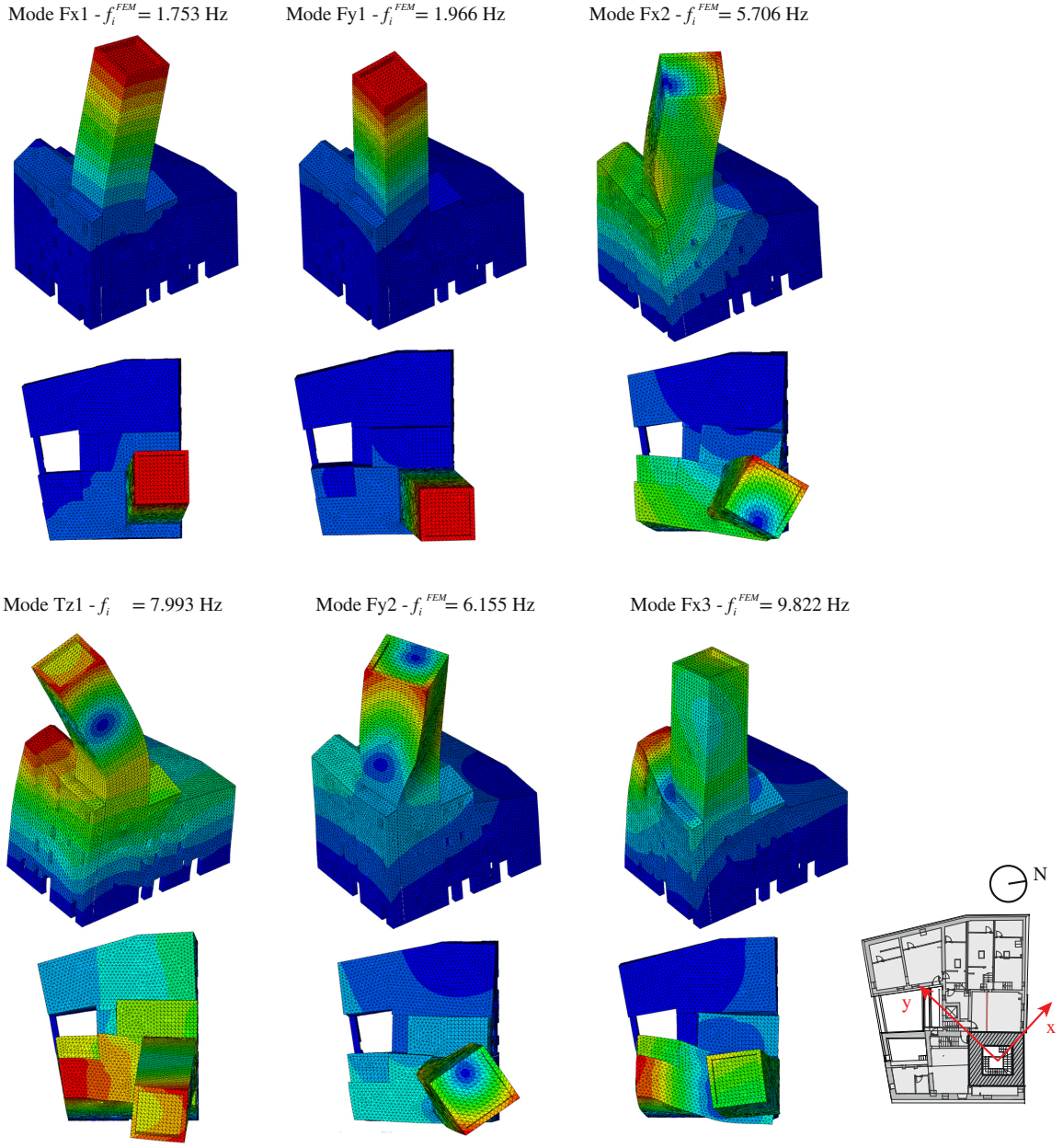

Figure 7: Numerical mode shapes obtained by linear modal analysis of the tuned FEM of the Sciri Tower.

4.4. Comparison of surrogate models

In order to compare the accuracy of the surrogate models previously introduced in Section 2, the training population must be generated on the basis of the numerical FEM. To this end, the design space must be uniformly sampled in the first place. Following the parametrization of the FEM into macro-elements, the stiffness coefficients k_i, $i = 1, ..., 4$, have been defined as random variables with upper/lower limits of ±15%. Therefore, the design space $\mathbb{D}$ in Eq. (17) takes the form of:

$$\mathbb{D} = \left\{ \mathbf{x} \in \mathbb{R}^4 : -0.15 \leq k_i \leq 0.15 \right\}. \tag{20}$$

The quality of the sampling of the design space governs the accuracy of the surrogate models. In this work, random samples have been drawn uniformly over $\mathbb{D}$ using the quasi-random sequence of Sobol [44]. In order to select the size of the training population, a convergence analysis is carried out in Fig. 9. In particular, five different sample sizes have been selected, including $N = 64$, 128, 256, 512 and 1024 individuals. For comparison purposes, the largest population of 1024 samples is assumed as reference. The statistical analysis of the reference population is depicted in Figure 8. Specifically, Fig. 8 (a) presents the sampled data points of the design variables k_1 and k_2. It is noted in this figure that, in virtue of the quasi-random sequence of Sobol, the domain of definition of these variables is uniformly sampled. The analysis is further extended in Fig. 8 (b) where the histograms of the data samples k_i, $i = 1, ..., 4$, are presented. In all the cases, the histograms are almost flat, which proves the uniformity of the data sampling. On this basis, the first six natural frequencies and mode shapes have been obtained for all the training population sizes by the FEM of the Sciri Tower. Figures 8 (c) and (d) depict the probability density functions (PDF) and cumulative density functions (CDF) of the target natural frequencies, respectively.

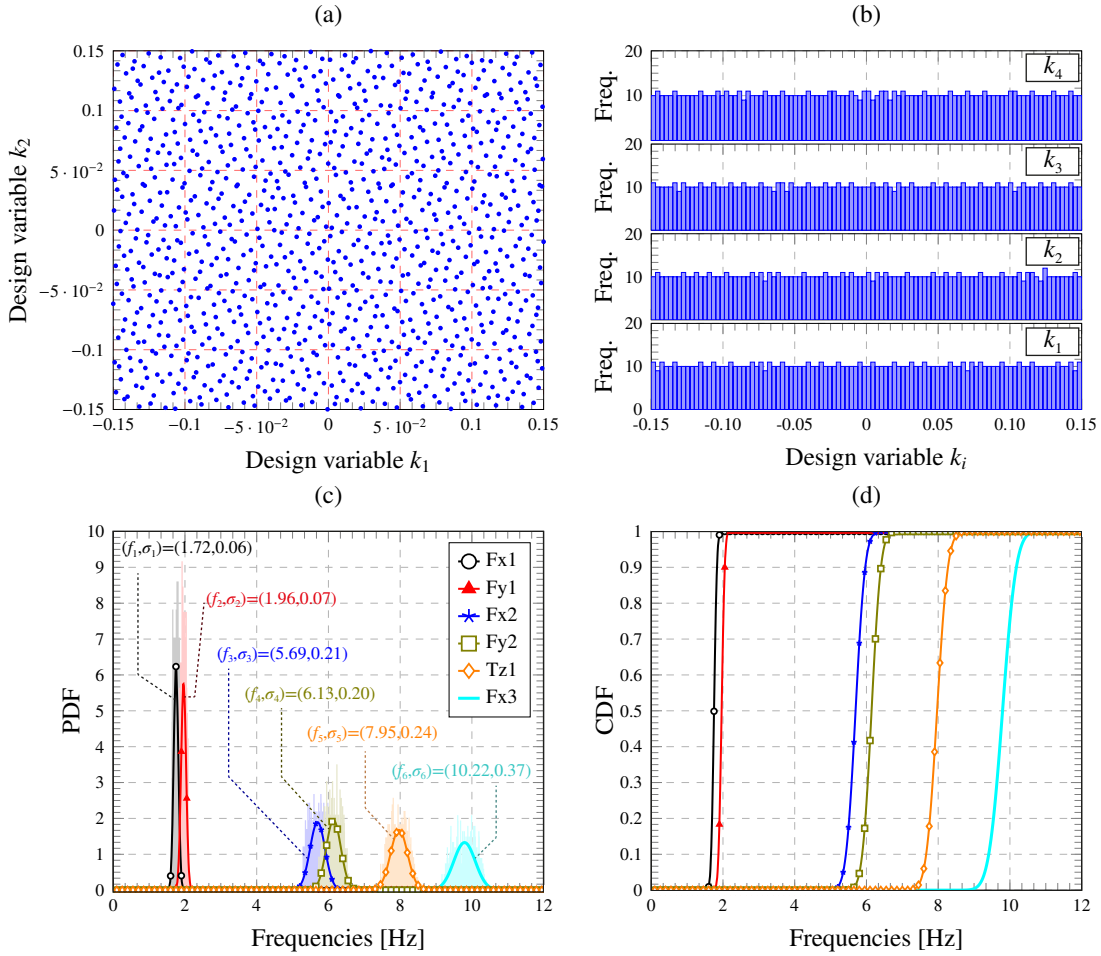

Figure 8: (a) Sampled data points of the design variables k_1 and k_2. (b) Histograms of the data samples k_i, $i = 1, ..., 4$. (c) Probability density functions (PDF) and Gaussian approximations, and (d) cumulative density functions (CDF) of the first six natural frequencies obtained with the FEM of the Sciri Tower (reference population of 1024 samples).

The comparison between the studied surrogate models is performed in Fig. 9 through the mean value of the cost function in Eq. (15) $\overline{J}$ defined as:

$$\overline{J} = \frac{1}{N}\sum_{i=1}^{N} J(\mathbf{x}_i), \tag{21}$$

where the data points $\mathbf{x}_i$ correspond to the reference population ($N = 1024$ individuals), and the terms ε_i and δ_i in Eq. (16) are obtained by comparing the FEM estimates and the surrogate models for increasing training population sizes. Therefore, a value of $\overline{J} = 0$ indicates a perfect fitting of the estimates of the FEM by the surrogate model, while larger values of $\overline{J}$ evidence disagreements between their estimates. It is important to note that the regularization term in Eq. (15) has been omitted in this analysis ($\eta = 0$). In addition, in order to deepen into the comparison analysis, a second parameter variation range of ±100% has been also considered (variation ranges are denoted as quantities in parentheses in Fig. 9). Note that, although such a wide variation range results impractical for model updating applications, it provides a limit case to delve into the comparison of the surrogate models. The comparison between the surrogate models is conducted for different combinations of the weighting coefficients α and β, including solely the contribution of natural frequencies (α=1 and β=0 in Figs. 9 (a) and (d)), mode shapes (α=0 and β=1 in Figs. 9 (b) and (e)), and their combined contribution (α=1 and β=1 in Figs. 9 (c) and (f)). Let us first focus on the small parameter variation range of ±15% ((a), (b) and (c)). It is observed that the errors related to the MAC values dominate over the objective function (see Fig. (b)). This fact evidences that, for small variations in the parameters as it is the case of environmental effects or early-stage damage, the accurate fitting of variations in the mode shapes plays a dominant role in the structural assessment. With regard to the comparison between the surrogate models, the Kriging, RSM and RS-HDMR models are shown to provide approximations in decreasing order of accuracy. In particular, the RS-HDMR model provides unstable solutions for small training population sizes due to errors stemming from the Monte Carlo integration of the component functions (see Eq. (13)). In the case of the RSM model, little improvements are noted for increasing population sizes. This fact indicates that, for a low range of parameter variation, the response surfaces of the structure can be accurately captured by a quadratic expansion and, therefore, a low number of training samples suffice to build an accurate meta-model. Finally, it is noted that the accuracy of the Kriging model monotonically increases with the training population size. Specifically, it is noted that $\overline{J}$ reaches zero at the reference population. This behaviour can be explained by the definition of the Kriging predictor in Eq. (5), where the regression term $y_r(\mathbf{x})$ forces the model to exactly reproduce all the sampled data.

Some differences can be observed for the large parameter variation range in Figs. 9 (c), (d) and (f). Firstly, it is noted that the errors stemming from the modelling of the frequencies and mode shapes are similar. In light of the previous analysis, it can be concluded that model updating approaches only considering resonant frequency shifts can be used to identify large stiffness variations, while their applicability to identify low damage levels may be limited. With regard to the comparison between the surrogate models, the Kriging, RS-HDMR, and RSM models are shown to provide approximations in decreasing order of accuracy. A closer inspection reveals that the RSM reaches an asymptotic value at 512 individuals from which no more improvements are found. The tendency of the RS-HDMR model is similar, although it exhibits faster convergence rates and an asymptotic limit at larger sampling sizes. These similarities result from the fact that both models are based upon a polynomial expansion of the response. In addition, given that the RS-HDMR considers orthonormal polynomials with higher order, the asymptotic limit is reached in this case at a larger sampling size. Finally, the Kriging model initially exhibits slower convergence rates (see e.g. Fig. 9 (d)), although its accuracy for moderate and large sampling sizes outperforms that of the other two surrogate models. In view of these results, a training population size of 512 individuals is selected in all the subsequent analyses.

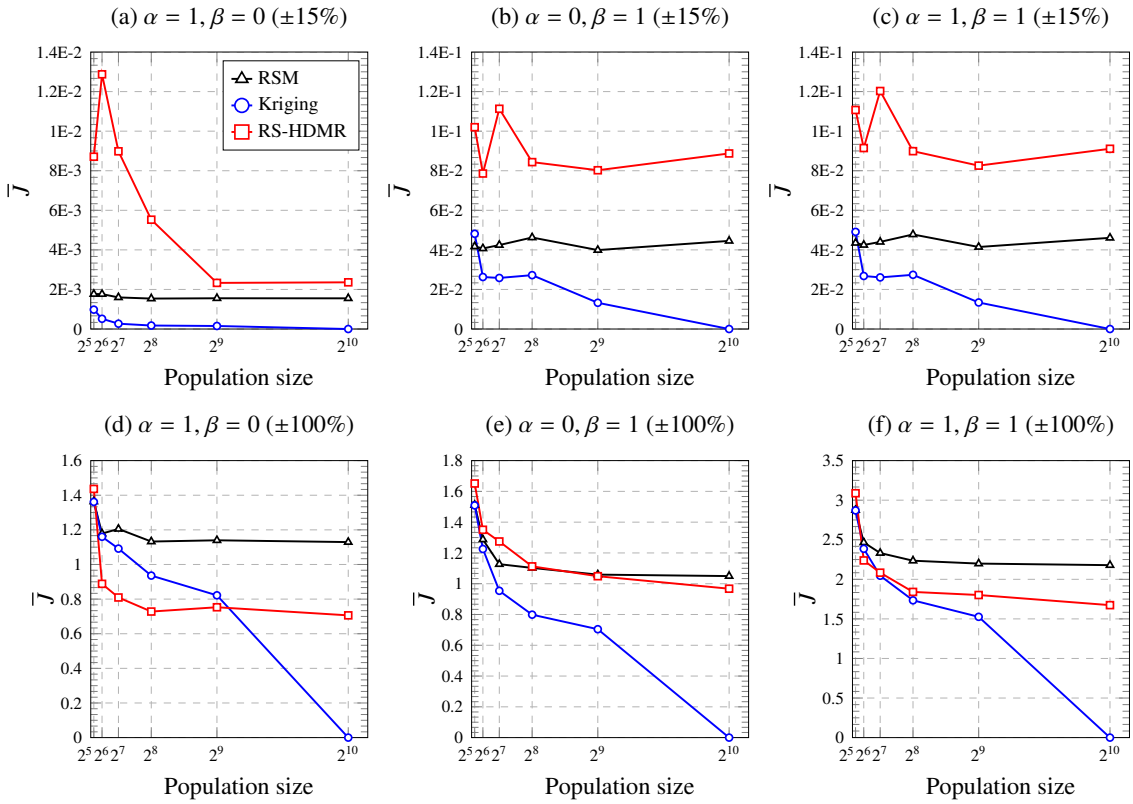

Figure 9: Mean value of the objective function ($\overline{J}$) versus training population size (reference population of 1024 samples).

Figure 10 shows a scatter plot describing the relationship between the original FEM and the surrogate models for the first natural frequency. In the case of a low parameter variation range of ±15% (Figs. 10 (a), (b) and (c)), the low scatter of the points around the diagonal line corroborates that the surrogate models are formed with accuracy. Conversely, in the case of a large parameter variation range of ±100% (Figs. 10 (d), (e) and (f)), the notable scatter around the diagonal line indicates the existence of considerable discrepancies between the models. Tables 4 and 5 present the comparative study between the direct MCS and the surrogate models for max/min values, mean values, standard deviation (σ) and coefficient of determination (R^2) for the first three natural frequencies, considering parameter variation ranges of ±15% and ±100%, respectively. Firstly, it is observed in Table 4 that, despite the differences previously reported in Fig. 9, all the surrogate models yield estimates very proximate to the MCS with coefficients of determination very close to one. On the other hand, larger discrepancies can be observed in Table 5 for the case of a large parameter variation range of ±100%. Specifically, large disagreements are found in all the surrogate models for minimum frequency values (severe damage) as also evidenced by the scatters in Figure 10. It is concluded from this analysis that the training population size and the surrogate models must be properly tailored according to the expected damage level. In particular, and in light of the previously reported results in Figs. 9 (a), (b) and (c), the order of the polynomial expansion involved in the RSM and the RS-HDMR models must be adequately selected according to the desired variability of the parameters. That is to say, wider definition domains of the parameters require polynomial functions with increasing orders and larger training population sizes. Conversely, the Kriging model offers a more flexible solution in the sense that its capability to approach wider variability domains is directly determined by the size of the training population.

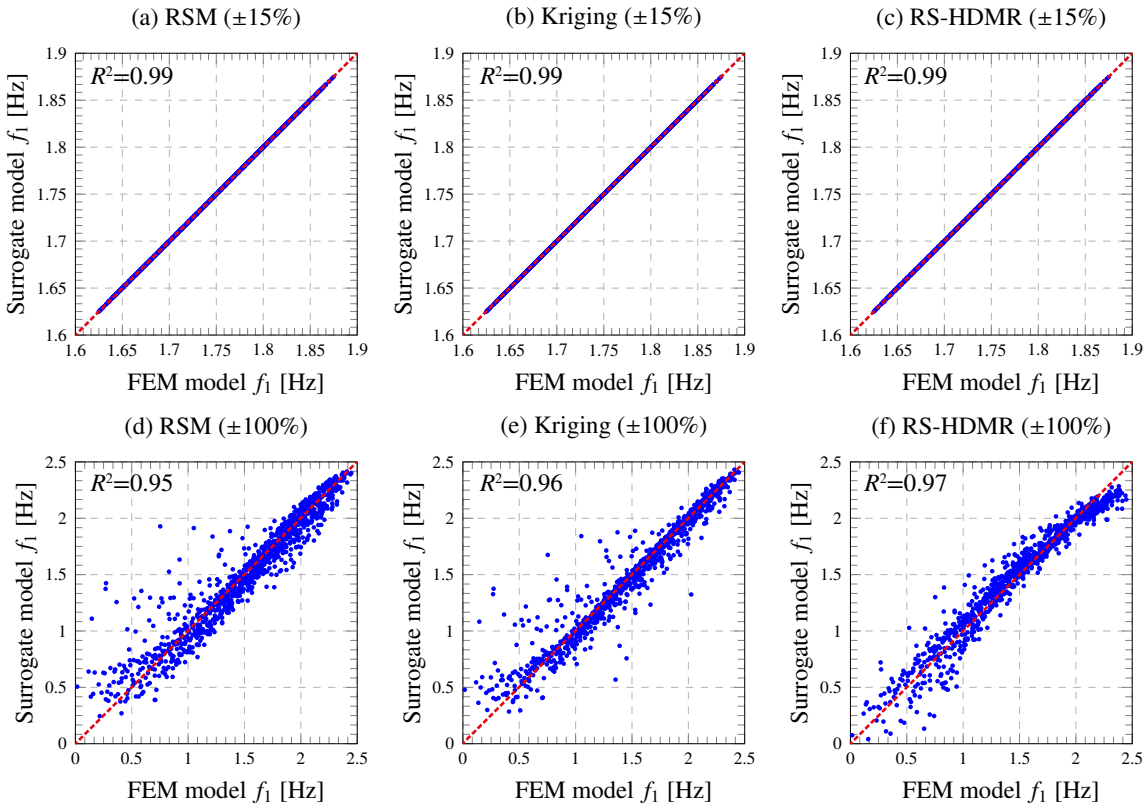

Figure 10: Scatter plot of RSM (a,d), Kriging (b,e) and RS-HDMR (c,f) surrogate models with respect to the 3D FEM of the Sciri Tower for the first natural frequency (f_1) (training population of 512 samples and reference population of 1024 samples).

Table 4: Comparative study between MCS (1024 samples) and RSM, Kriging, and RS-HDMR models (512 samples) for maximum/minimum values, standard deviations (σ), and coefficients of determination (R^2) for the first three natural frequencies and ±15% parameter variation.

Mode 1					
	MC	RSM	Kriging	RS-HDMR	Diff [%]
Min. Val. [Hz]	1.6248	1.6248	1.6248	1.6247	-0.0030 \ -0.0029 \ 0.0044
Max. Val. [Hz]	1.8748	1.8747	1.8747	1.8746	0.0044 \ 0.0028 \ 0.0123
Mean [Hz]	1.7502	1.7502	1.7502	1.7502	-0.0001 \ -0.0002 \ -0.0001
SD [Hz] (σ)	0.0640	0.0640	0.0640	0.0640	-0.0024 \ -0.0050 \ -0.0019
R^2	-	0.9990	0.9990	0.9990	-

Mode 2					
	MC	RSM	Kriging	RS-HDMR	Diff [%]
Min. Val. [Hz]	1.8237	1.8238	1.8237	1.8241	-0.0029 \ 0.0019 \ -0.0246
Max. Val. [Hz]	2.1009	2.1009	2.1010	2.1007	0.0004 \ -0.0029 \ 0.0088
Mean [Hz]	1.9620	1.9620	1.9620	1.9620	0.0000 \ -0.0001 \ 0.0000
SD [Hz] (σ)	0.0687	0.0687	0.0687	0.0687	0.0011 \ -0.0029 \ 0.0027
R^2	-	0.9990	0.9990	0.9990	-

Mode 3					
	MC	RSM	Kriging	RS-HDMR	Diff [%]
Min. Val. [Hz]	5.2936	5.2941	5.2935	5.2938	-0.0102 \ 0.0017 \ -0.0045
Max. Val. [Hz]	6.0975	6.0972	6.0975	6.0970	0.0042 \ -0.0002 \ 0.0079
Mean [Hz]	5.6966	5.6966	5.6966	5.6966	0.0000 \ -0.0001 \ 0.0000
SD [Hz] (σ)	0.2104	0.2104	0.2105	0.2104	0.0003 \ -0.0021 \ 0.0006
R^2	-	0.9990	0.9990	0.9990	-

Table 5: Comparative study between MCS (1024 samples) and RSM, Kriging, and RS-HDMR models (512 samples) for maximum/minimum values, standard deviations (σ), and coefficients of determination (R^2) for the first three natural frequencies and ±100% parameter variation.

Mode 1					
	MC	RSM	Kriging	RS-HDMR	Diff [%]
Min. Val. [Hz]	0.016	0.245	0.285	-0.451	-1432.206 \ -1683.563 \ 2925.280
Max. Val. [Hz]	2.447	2.415	2.431	2.284	1.327 \ 0.667 \ 6.680
Mean [Hz]	1.508	1.505	1.509	1.505	0.191 \ -0.081 \ 0.197
SD [Hz] (σ)	0.529	0.503	0.506	0.521	4.861 \ 4.351 \ 1.455
R^2	-	0.951	0.963	0.967	-
Mode 2					
	MC	RSM	Kriging	RS-HDMR	Diff [%]
Min. Val. [Hz]	0.018	0.269	0.313	-0.462	-1360.629 \ -1600.225 \ 2613.861
Max. Val. [Hz]	2.737	2.705	2.723	2.638	1.168 \ 0.514 \ 3.616
Mean [Hz]	1.671	1.668	1.673	1.668	0.165 \ -0.107 \ 0.172
SD [Hz] (σ)	0.586	0.557	0.559	0.578	5.012 \ 4.582 \ 1.429
R^2	-	0.949	0.962	0.966	-
Mode 3					
	MC	RSM	Kriging	RS-HDMR	Diff [%]
Min. Val. [Hz]	0.052	0.753	0.915	-2.276	-1356.476 \ -1671.808 \ 4504.251
Max. Val. [Hz]	7.934	7.895	7.953	7.337	0.490 \ -0.246 \ 7.522
Mean [Hz]	4.825	4.817	4.830	4.817	0.162 \ -0.096 \ 0.169
SD [Hz] (σ)	1.739	1.622	1.635	1.714	6.686 \ 5.944 \ 1.413
R^2	-	0.929	0.947	0.958	-

Finally, it is important to compare the surrogate models in terms of computational times. While the mean computational time needed to perform a modal analysis of the 3D FEM amounts to about 7 minutes, the evaluation times of the RSM, Kriging and RS-HDMR models are about 3.2 ms, 7.2 ms, and 142 ms, respectively. These reductions provide an efficient and affordable solution to conduct the multiple function evaluations involved in most heuristic optimization algorithms. Specifically, in the case of long-term continuous SHM applications, the computation time involved in the system identification and model updating cannot exceed the signal acquisition times for real-time structural assessment. In the case of complex historic structures, the limited computing capacity of most current computers makes the use of surrogate models the only feasible solution for that purpose.

4.5. Surrogate-based continuous structural assessment of the Sciri Tower

In this section, the surrogate-based continuous structural assessment approach previously presented in Section 3 is applied to the case study of the Sciri Tower. In particular, the analyses focus on the capability of the studied surrogate models to assess the sensibility of the elastic properties of the macro-elements M_i, $i = 1, ..., 4$, to environmental temperature fluctuations. Figure 11 shows the time histories of the natural frequencies of the first six modes of the tower continuously identified by A-OMA and tracked throughout the monitoring period since 13$^{\text{th}}$ February until 10$^{\text{th}}$ March 2019. In this figure, the temperature time series recorded by the two thermocouples (indoor and outdoor) are also shown. It is clearly noted that the identified natural frequencies exhibit a positive correlation with temperature, that is, increases in temperature lead to increasing natural frequencies. This effect is frequently observed in masonry structures, where the thermal expansion of masonry originates the closure of superficial cracks or micro-cracks, as well as minor discontinuities in the structure (see e.g. [8, 9, 12, 45]).

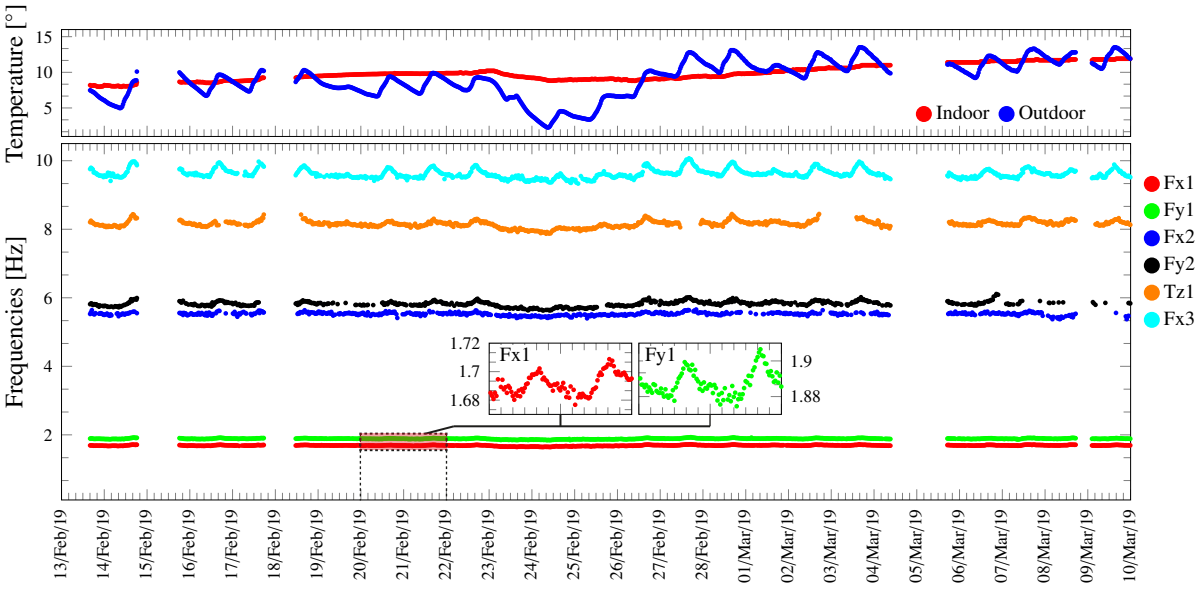

Figure 11: Temperature time series and frequency tracking in the Sciri Tower since 13th February until 10th March 2019.

Based upon the system identification results in Fig. 11, the surrogate-based model updating has been solved continuously for each set of identified modal data (30 min). In this case, the regularization term in Eq. (15) has been included ($\eta = 0.3$). To do so, the reference vector of design variables $\mathbf{x}^0$ has been defined as $\mathbf{x}^0 = [0, 0, 0, 0]^T$ ($k_i = 0, i = 1, ..., 4$), that is the nominal values of the Young's moduli of the macro-elements M_i. Moreover, in order to accurately capture the small stiffness variations induced by temperature effects, a parameter variation range of $\pm 15\%$ has been considered. The resulting non-linear minimization problem in Eq. (17) has been iteratively solved using a Particle Swarm optimization algorithm and weighting parameters $\alpha = \beta = 1$. In addition, the mode shapes of modes Fx2 and Fy2 have been excluded from the objective function $J(\mathbf{X})$ because of their high complexity level as previously shown in Fig. 4. Figure 12 shows the time series of the identified Young's moduli E_i of the sections of the tower included in the macro-elements M_i by using the RSM, Kriging and RS-HDMR meta-models. Let us recall that the building aggregate is constituted by different materials, all of them affected by the stiffness coefficient k_1. Nevertheless, for clarity purposes, only the elastic moduli corresponding to the tower are reported herein. In order to further investigate the sensitivity of E_i to environmental temperature, Fig. 13 depicts E_i versus mean environmental temperature (indoor and outdoor). It is noted that all the surrogate models report lower stiffness in the first two macro-elements (M_1 and M_2), and a stiffness value about 7% larger in the last two macro-elements (M_3 and M_4). Furthermore, it is clearly observed that the temperature sensitivities decrease with height. This behaviour can be ascribed to the closure of micro-cracks induced by thermal expansion, which presumably causes a stronger effect on those regions of the structure where expansion is more constrained, that is close to the base, and where the material is more heterogeneous. Conversely, the macro-elements of the upper part of the tower are more free to expand and the contribution of crack closure to the effective stiffness is less influential. It is interesting to note that, despite the similarities between the surrogate models for a parameter variation range of $\pm 15\%$ reported in the previous section, some differences are noticeable. In particular, it is observed that the elastic modulus of the top macro-element M_4 identified by the RSM and the HD-RSMR models has almost no sensitivity to temperature variations (see Fig. 13 (a) and (c)). This is not the case of the results obtained by the Kriging model which do show some small temperature sensibility in the macro-element M_4 (Fig. 13 (b)).

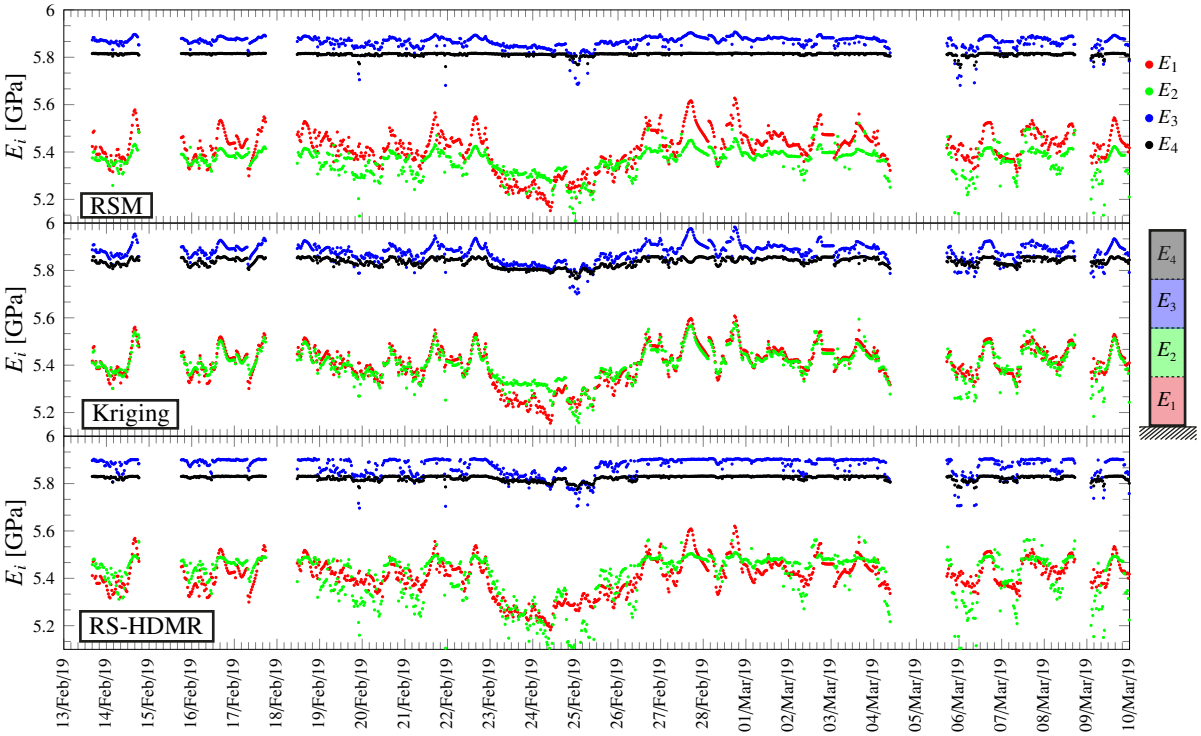

Figure 12: Time series of updated Young's moduli E_i of the sections of the Sciri Tower included in the macro-elements M_i, $i = 1, ..., 4$, using the RSM, Kriging and RS-HDMR meta-models.

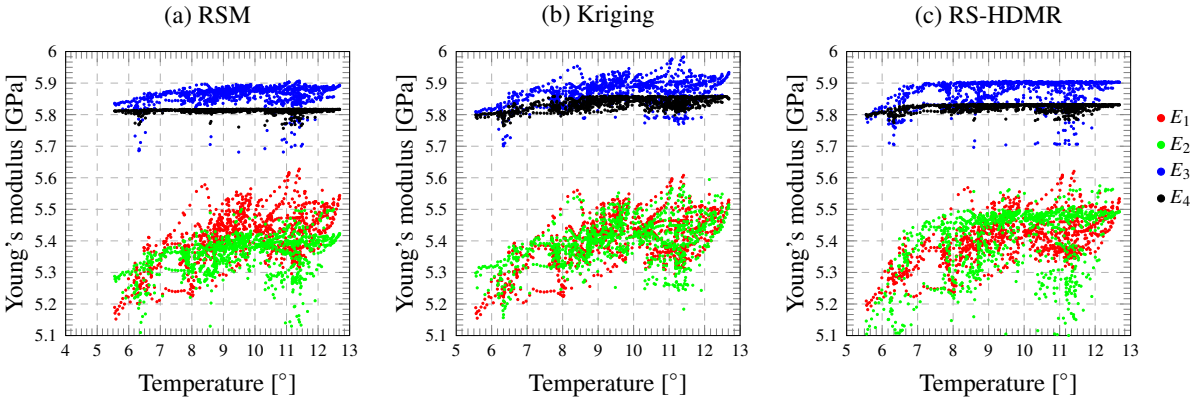

Figure 13: Updated Young's moduli E_i of the sections of the Sciri Tower included in the macro-elements M_i, $i = 1, ..., 4$, versus mean environmental temperature using the RSM, Kriging and RS-HDMR meta-models.

Finally, Fig. 14 and Table 6 evaluate the fitness of the studied surrogate models in terms of fitness of the natural frequencies and mode shapes. With regard to the modelling of the natural frequencies, it is observed in Fig. 14 that the errors ($\Delta f_i = f_i^{\text{exp}} - f_i^{\text{FEM}}$) exhibit an approximately constant mean. This fact evidences some modelling limitations of the FEM to accurately reproduce the experimental data, specially the resonant frequencies of high order models such as Fy2, Tz1 and Fx3. It is also interesting to note that the differences between experimental and numerical values exhibit oscillations related to daily temperature variations. This indicates that some of the sensitivity of the structure to temperature fluctuations is not well captured by the surrogate models. This may be due to errors related to the accuracy of the surrogate models, as well as intrinsic limitations of the selected FEM parametrization. For instance, the cooling and heating cycles of the structure are chiefly related to the sun's trajectory, which may not be accurately represented by variations of the elastic moduli of the defined macro-elements. With regard to the *MAC* values between the experimental and numerical mode shapes, quite stable values above 0.8 are noted in Fig. 14. The results reported in Table 6 offer a global evaluation of the fitness of the surrogate models. While only limited differences are found as expected from the analyses of the previous section, it is noted that the Kriging model provides better results for modes Tz1 and Fx3. This explains the better

performance of this model for representing the temperature sensitivity of the top macro-element as previously shown in Fig. 13. All things considered, it is concluded that the Kriging model features a superior capacity for the continuous surrogate-based model updating of historic structures, followed by the RSM and RS-HDMR models in decreasing order of accuracy.

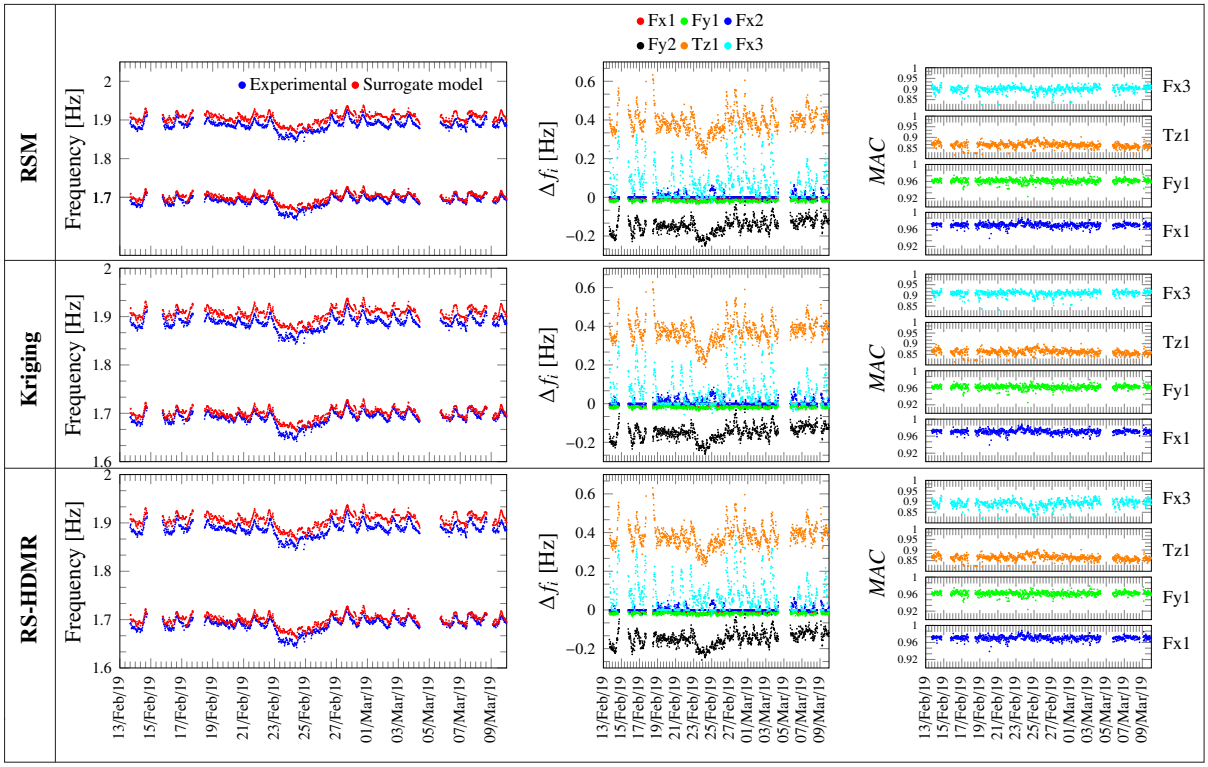

Figure 14: Analysis of the fitness of the RSM, Kriging and RS-HDMR surrogate models in terms of natural frequencies and mode shapes throughout the monitoring period since 13$^{\text{th}}$ February until 10$^{\text{th}}$ March 2019 ($\Delta f_i = f_i^{\text{exp}} - f_i^{\text{surr}}$).

Table 6: Comparison of the RSM, Kriging and RS-HDMR surrogate models in terms of mean differences between experimental and numerical natural frequencies and mode shapes throughout the monitoring period since 13$^{\text{th}}$ February until 10$^{\text{th}}$ March 2019.

Mode	RSM		Kriging		RS-HDMR	
	$\frac{\lvert f_i^{\text{exp}} - f_i^{\text{surr}} \rvert}{f_i^{\text{exp}}}$ [%]	MAC_i	$\frac{\lvert f_i^{\text{exp}} - f_i^{\text{surr}} \rvert}{f_i^{\text{exp}}}$ [%]	MAC_i	$\frac{\lvert f_i^{\text{exp}} - f_i^{\text{surr}} \rvert}{f_i^{\text{exp}}}$ [%]	MAC_i
Fx1	0.475	0.971	0.453	0.971	0.483	0.971
Fy1	0.938	0.962	0.974	0.962	0.969	0.962
Fx2	0.102	-	0.158	-	0.095	-
Fy2	2.504	-	2.560	-	2.514	-
Tz1	4.758	0.863	4.581	0.860	4.680	0.863
Fx3	0.722	0.899	0.600	0.910	0.670	0.890
Mean	**1.583**	**0.924**	**1.554**	**0.926**	**1.569**	**0.921**

5. Conclusions

This paper has presented an innovative surrogate-based model updating approach for real-time structural assessment of historical buildings. The methodology has been validated considering the case study of the Sciri Tower located in the city of Perugia (Italy). Three different surrogate models have been considered, namely the RSM, Kriging, and RS-HDMR models, and their effectiveness has been compared from an SHM perspective through regression analysis of their estimates of the modal features against those obtained by a numerical model. To do so, a fully detailed 3D FEM of the tower and the adjoining building has been built and parametrized through four macro-elements with parametric elastic properties. On this basis, different training populations with increasing sizes have been generated by Monte Carlo simulations in order to evaluate the robustness and accuracy of the

considered surrogate models. Finally, their capability to continuously assess the condition of the Sciri Tower has been also analysed. With this purpose, a continuous AVT has been conducted since 13th February until 10th March 2019 and the modal features of the structure have been identified by A-OMA. Afterwards, the design parameters (equivalent elastic properties of macro-elements) have been continuously fitted by minimizing the mismatch between the identified modal features and the estimates of the surrogate models. The key findings of this work can be summarized as follows:

- Cost functions in the model updating involving both natural frequencies and mode shapes are essential to determine small stiffness variations related to environmental effects or early-stage damage.
- The studied surrogate models offer efficient and affordable solutions for real-time surrogate-based structural assessment of historic structures. Specifically, the mean computational time needed to perform a modal analysis of the 3D FEM of the Sciri Tower amounts to about 7 minutes, while the evaluation computational times of the RSM, Kriging and RS-HDMR models drop to about 3.2 ms, 7.2 ms, and 142 ms, respectively.
- The temperature sensitivity of the Sciri Tower can be modelled by means of localized variations in the elastic moduli of macro-elements discretizing the FEM.
- The temperature sensitivity of equivalent elastic parameters of the tower decreases with height. This behaviour has been ascribed to the closure of micro-cracks induced by thermal expansion, which may cause a stronger effect on those regions of the structure where masonry is more heterogeneous and has larger width, or where volume expansion is more constrained, that is, close to the base.
- The presented results have demonstrated that the surrogate models can accurately reproduce the positive correlation of the resonant frequencies of the tower with the environmental temperature. Furthermore, the Kriging model has proved to be superior for reproducing the low temperature sensitivities of macro-elements located in the uppermost part of the tower.

Acknowledgement

This work was supported by the Italian Ministry of Education, University and Research (MIUR) through the funded project of national interest "SMART-BRICK: novel strain-sensing nanocomposite clay brick enabling self-monitoring masonry structures" (Protocol No. 2015M55L27).

[1] G. Bartoli, M. Betti, S. Monchetti, Seismic risk assessment of historic masonry towers: comparison of four case studies, Journal of Performance of Constructed Facilities 31 (2017) 04017039.
[2] D. F. D'Ayala, S. Paganoni, Assessment and analysis of damage in L'Aquila historic city centre after 6th April 2009, Bulletin of Earthquake Engineering 9 (2011) 81–104.
[3] F. Meroni, T. Squarcina, V. Pessina, M. Locati, M. Modica, R. Zoboli, A Damage Scenario for the 2012 Northern Italy Earthquakes and Estimation of the Economic Losses to Residential Buildings, International Journal of Disaster Risk Science 8 (2017) 326–341.
[4] C. Liu, Y. Zheng, Z. Xie, X. Xiong, Rupture features of the 2016 Mw 6.2 Norcia earthquake and its possible relationship with strong seismic hazards, Geophysical Research Letters 44 (2017) 1320–1328.
[5] M. G. Masciotta, L. F. Ramos, P. B. Lourenço, The importance of structural monitoring as a diagnosis and control tool in the restoration process of heritage structures: a case study in Portugal, Journal of Cultural Heritage 27 (2017) 36–47.
[6] E. Mesquita, A. Arêde, N. Pinto, P. Antunes, H. Varum, Long-term monitoring of a damaged historic structure using a wireless sensor network, Engineering Structures 161 (2018) 108–117.
[7] F. Ceroni, M. Pecce, S. Voto, G. Manfredi, Historical, architectural, and structural assessment of the Bell Tower of Santa Maria del Carmine, International Journal of Architectural Heritage 3 (2009) 169–194.
[8] A. Saisi, C. Gentile, M. Guidobaldi, Post-earthquake continuous dynamic monitoring of the Gabbia Tower in Mantua, Italy, Construction and Building Materials 81 (2015) 101–112.
[9] R. M. Azzara, G. De Roeck, M. Girardi, C. Padovani, D. Pellegrini, E. Reynders, The influence of environmental parameters on the dynamic behaviour of the San Frediano bell tower in Lucca, Engineering Structures 156 (2018) 175–187.
[10] M. L. Pecorelli, R. Ceravolo, R. Epicoco, An automatic modal identification procedure for the permanent dynamic monitoring of the sanctuary of Vicoforte, International Journal of Architectural Heritage (2018) 1–15.

[11] F. Ubertini, N. Cavalagli, A. Kita, G. Comanducci, Assessment of a monumental masonry bell-tower after 2016 Central Italy seismic sequence by long-term SHM, Bulletin of Earthquake Engineering 16 (2018) 775–801.
[12] C. Gentile, A. Ruccolo, A. Saisi, Continuous dynamic monitoring to enhance the knowledge of a historic bell-tower, International Journal of Architectural Heritage (2019) 1–13.
[13] S. Atamturktur, J. A. Laman, Finite element model correlation and calibration of historic masonry monuments, The Structural Design of Tall and Special Buildings 21 (2012) 96–113.
[14] A. C. Altunişik, F. Y. Okur, A. F. Genç, M. Günaydin, S. Adanur, Automated model updating of historical masonry structures based on ambient vibration measurements, Journal of Performance of Constructed Facilities 32 (2017) 04017126.
[15] C. Gentile, A. Saisi, A. Cabboi, Structural identification of a masonry tower based on operational modal analysis, International Journal of Architectural Heritage 9 (2015) 98–110.
[16] W. H. Chen, Z. R. Lu, W. Lin, S. H. Chen, Y. Q. Ni, Y. Xia, W. Y. Liao, Theoretical and experimental modal analysis of the Guangzhou New TV Tower, Engineering Structures 33 (2011) 3628–3646.
[17] S. Sehgal, H. Kumar, Structural dynamic model updating techniques: A state of the art review, Archives of computational methods in engineering 23 (2016) 515–533.
[18] M. Friswell, J. E. Mottershead, Finite element model updating in structural dynamics, volume 38, Springer Science & Business Media, 2013.
[19] J. Magalhães-Mendes, D. Greiner, Evolutionary algorithms and metaheuristics in civil engineering and construction management, volume 39, Springer, 2015.
[20] N. Cavalagli, G. Comanducci, F. Ubertini, Earthquake–induced damage detection in a monumental masonry bell-tower using long-term dynamic monitoring data, Journal of Earthquake Engineering 22 (2018) 96–119.
[21] C. Gentile, N. Gallino, Ambient vibration testing and structural evaluation of an historic suspension footbridge, Advances in Engineering Software 39 (2008) 356–366.
[22] L. F. Ramos, P. B. Lourenço, G. De Roeck, A. Campos-Costa, Damage identification in masonry structures with vibration measurements, Structural Analysis of Historic Construction: Preserving Safety and Significance, Vols 1 and 2 (2008) 311–319.
[23] A. C. Altunişik, F. Y. Okur, A. Genç, M. Günaydin, O. Karahasan, Automated model updating effect on the linear and nonlinear dynamic responses of historical masonry structures, Experimental Techniques 42 (2018) 605–621.
[24] P. Pachón, R. Castro, E. García-Macías, V. Compan, E. Puertas, E. Torroja's bridge: Tailored experimental setup for SHM of a historical bridge with a reduced number of sensors, Engineering Structures 162 (2018) 11–21.
[25] A. Cabboi, C. Gentile, A. Saisi, From continuous vibration monitoring to FEM-based damage assessment: application on a stone-masonry tower, Construction and Building Materials 156 (2017) 252–265.
[26] L. Vincenzi, M. Savoia, Coupling response surface and differential evolution for parameter identification problems, Computer–Aided Civil and Infrastructure Engineering 30 (2015) 376–393.
[27] S. Qin, Y. Zhang, Y. L. Zhou, J. Kang, Dynamic model updating for bridge structures using the kriging model and PSO algorithm ensemble with higher vibration modes, Sensors 18 (2018) 1879.
[28] W. Torres, J. L. Almazán, C. Sandoval, R. Boroschek, Operational modal analysis and FE model updating of the Metropolitan Cathedral of Santiago, Chile, Engineering Structures 143 (2017) 169–188.
[29] E. Bassoli, L. Vincenzi, A. M. D'Altri, S. de Miranda, M. Forghieri, G. Castellazzi, Ambient vibration–based finite element model updating of an earthquake–damaged masonry tower, Structural Control and Health Monitoring 25 (2018) e2150.
[30] R. H. Myers, D. C. Montgomery, C. M. Anderson-Cook, Response surface methodology: process and product optimization using designed experiments, John Wiley & Sons, 4th edition, 2016.
[31] I. Venanzi, A. Kita, N. Cavalagli, L. Ierimonti, F. Ubertini, Continuous OMA for Damage Detection and Localization in the Sciri tower in Perugia, Italy, in: Proceedings of the 8th International Operational Modal Analysis Conference (IOMAC), Copenhagen, Denmark, 2019.
[32] Z. H. Han, K. S. Zhang, Surrogate-based optimization, in: Real-world applications of genetic algorithms, IntechOpen, 2012.
[33] G. Matheron, Principles of geostatistics, Economic geology 58 (1963) 1246–1266.
[34] S. N. Lophaven, H. B. Nielsen, J. Søndergaard, DACE-A Matlab Kriging toolbox, version 2.0, Technical Report, 2002.
[35] H. Rabitz, Ö. F. Aliş, General foundations of high-dimensional model representations, Journal of Mathematical Chemistry 25 (1999) 197–233.
[36] T. Ziehn, A. Tomlin, GUI-HDMR - a software tool for global sensitivity analysis of complex models,

Environmental Modelling & Software 24 (2009) 775–785.
[37] T. Ziehn, A. Tomlin, Global sensitivity analysis of a 3d street canyon model-part i: The development of high dimensional model representations, Atmospheric Environment 42 (2008) 1857–1873.
[38] I. M. Sobol, Global sensitivity indices for nonlinear mathematical models and their Monte Carlo estimates, Mathematics and Computers in Simulation 55 (2001) 271–280.
[39] G. Li, H. Rabitz, S. W. Wang, P. G. Georgopoulos, Correlation method for variance reduction of Monte Carlo integration in RS-HDMR, Journal of Computational Chemistry 24 (2003) 277–283.
[40] G. Li, H. Rabitz, Ratio control variate method for efficiently determining high-dimensional model representations, Journal of Computational Chemistry 27 (2006) 1112–1118.
[41] F. Magalhães, Á. Cunha, Explaining operational modal analysis with data from an arch bridge, Mechanical Systems and Signal Processing 25 (2011) 1431–1450.
[42] R. S. Pappa, K. B. Elliott, A. Schenk, Consistent-mode indicator for the eigensystem realization algorithm, Journal of Guidance, Control, and Dynamics 16 (1993) 852–858.
[43] I. Venanzi, D. Salciarini, C. Tamagnini, The effect of soil-foundation-structure interaction on the wind-induced response of tall buildings, Engineering Structures 79 (2014) 117–130.
[44] I. M. Sobol, On the distribution of points in a cube and the approximate evaluation of integrals, Zhurnal Vychislitel'noi Matematiki i Matematicheskoi Fiziki 7 (1967) 784–802.
[45] F. Ubertini, G. Comanducci, N. Cavalagli, A. L. Pisello, A. L. Materazzi, F. Cotana, Environmental effects on natural frequencies of the San Pietro bell tower in Perugia, Italy, and their removal for structural performance assessment, Mechanical Systems and Signal Processing 82 (2017) 307–322.